Proceedings of the 7th International Conference on Theoretical and Applied Nanoscience and Nanotechnology (TANN'23)
Canada – June 01-03, 2023
Paper No. 112
DOI: 10.11159/tann23.112

High-Performance Csgebr$_3$ Perovskite/ WS_2 Nano-Flakes Field-Effect Transistor In Vacuum

Y. Rezaei Nik[1*], A. Reyhani[2], S. Farjami-Shayesteh[1], S.Z. Mortazavi[2], R. Karimi[3], and M. Teimouri [4]
[1]Department of Physics, University of Guilan, P.O. Box 4199613776, Rasht, Iran.
yousefrezaeinik@gmail.com; saber@guilan.ac.ir
[2]Physics Dept., Faculty of Science, Imam Khomeini International University, P.O. Box 34149-16818, Qazvin, Iran
reyhani@sci.ikiu.ac.ir; Z.Mortazavi@sci.ikiu.ac.ir
[3]Department of Physics and Astronomy, University of Waterloo, 200 University Avenue West Waterloo, Ontario, Canada
r3karimi@uwaterloo.ca
[4]Mathematical Dept, Faculty of Science, Imam Khomeini International University, P.O. Box 34149-16818, Qazvin, Iran
teimouri.masoumeh54@gmail.com

Abstract **-** In this research, due to the non-toxic nature of inorganic perovskite $CsGeBr_3$ (CGB), this material is applied to fabricate a CGB/WS_2 FET by drop-casting of lead free perovskite CGB on the WS_2 NFs FET. Then the electrical characterization of a hybrid lead free $CsGeBr_3$ perovskite/ WS_2 Nano-Flakes (NFs) Field-Effect transistor is investigated in ambient air and vacuum conditions with a simple back-gate device structure. The characterization of the fabricated device has been performed under the illumination of a laser source with a wavelength of ~532 nm and power of 9.13 $mWcm^{-2}$ out and inside the vacuum chamber at a constant pressure of $\sim 3\times10^{-3}$ mbar. By comparing devices in and out of vacuum. It is apparent that atmospheric adsorbates on CGB/WS_2 NFs FET degrade external quantum efficiency, photo-responsivity, and detectivity doubled and reached 2.9%, 0.012 AW^{-1}, and 4.15×106 Jones in comparison with the WS_2 NFs FET in the atmosphere. The results demonstrate that the observed shift in threshold voltage suggests the I_{ds} of the CGB/WS_2 NFs FET in vacuum conditions have increased compared to the WS_2-NFs FET in the atmosphere. Most importantly, the vacuum plays a significant role and shows the superior photo-sensing properties of the CGB/WS_2 NFs FET in vacuum are very promising to extend the hybrid heterostructure optoelectronic devices with excellent performance, especially in space.

Keywords**:** Field-Effect Transistor, $CsGeBr_3$, WS_2, Hetero-structure, vacuum

1. Introduction

Semiconductor photodetectors and transistor are used to convert the modulated light signal to the electrical domain, which have wide applications ranging from optical communication, and remote control to detection and image sensing [1–3]. Most appliances of photodetectors today adopt conventional inorganic materials such as Si, InGaAs, MoS_2 and especially WS_2, as a transition metal dichalcogenides (TMDCs), due to their unique properties, namely strong spin-orbit coupling, band splitting, good sensitivity and high robustness and high nonlinear susceptibility [4–9]. In recent decades, the 2D-TMDCs have received much interest to be applied in photonic applications that take advantage of variations in a material's band gap properties as a function of the 2D layer thickness [10–11]. However, some of the TMDCs nanomaterials have similar atomic structure and chemical behaviours like the 2D-WS_2 and MoS_2, but 2D-WS_2 has a much smaller effective electron mass in comparison to the latter one. Subsequently, transistors based on the 2D-WS_2 show a better performance rather than transistors based on the Si and MoS_2 due to its inert, non-toxic, and environmentally friendly properties [12–14]. In this context, all-inorganic perovskites $CsPbX_3$ (X = Cl, Br, I) also possess the large carrier diffusion length, low recombination of charge carriers, and demonstrating the great potential to be the next-generation active materials of photo-detectors at the aspects of low-cost, solution-processed, low-voltage operational features [15–21]. on the other hands, the lead base perovskites are toxic and dangerous for humans' health and may cause environmental damage because of its chemical stability [22–23]. To eliminate this problem, the $CsGeBr_3$ as a lead-free perovskite can be formed by replacing the lead component with germanium at the $CsPbX_3$ perovskite, which can detoxify the environment from the pollution of lead based perovskites and make these materials more environmentally friendly [24–26]. The performance of semiconductor heterojunction devices has markedly increased since the introduction of heterostructures. Perovskite heterostructure (PHS) devices are fabricated by combining semiconductors of varying bandgap energies such as the transition metal chalcogenides into a lattice of matching variables; these new structures are playing an increasingly important role in optoelectronics. It has been observed that when

heterogeneous materials are integrated many electronic and photo-electronic devices with high-performance properties can be created [2,22]. Some researches show that electrical transport properties were strongly affected by interfacial charged impurities, the adsorbates in ambient air adsorb on the surface or at the MoS_2/SiO_2 interface and affect not only the carrier transport behaviours but also the photoelectrical responses [27]. These adsorbates interact strongly with the MoS_2 film, resulting in the carrier scattering increase, and the decrease of the electron mobility, photoresponsivity, and gain. On the other hand, the adsorbates assist photocurrent relaxation and decrease the photocurrent decay times [28–30].

In this research, the performance of synthesized the CGB/WS_2 NFs Field-Effect-Transistors (FETs) is investigated under the illumination of the green laser with P= 9.13 $mWcm^{-2}$ as excitation power in ambient air and vacuum conditions. Optoelectronic properties of the devices such as external quantum efficiency, and photo-responsivity are measured and characterized. The optoelectronic measurements of the CGB/WS_2 NFs FET reveal a better performance in vacuum under illumination in comparison ambient air. summary, the effects of ambient air adsorption on the optoelectronic properties of a CGB/WS_2 NFs FET transistor are systematically studied. The results show that the adsorbates in ambient air adsorb on the surface. These adsorbates interact strongly with the surface of the device, resulting in the decrease of the photocurrent, photoresponsivity, and performance. In this study, the various characterization methods such as X-Ray Diffraction (XRD, and output and transfer characteristics are employed to evaluate the structure, performance and optoelectronic characteristics CGB/WS_2 FET transistor.

2. Experimental

2.1. Preparation of the WS_2 Nano–flakes

Figure.1 schematically illustrates our experimental Thermal Chemical Deposition Vapor TCVD set-up used in this work for the preparation of the WS_2-Nano Flakes. Prior to the growth the SiO_2/Si substrate and starting TCVD process for the furnace heating, the furnace is necessarily purged with Ar gas with a flow rate of ~ 450 sccm for 30 minutes for eliminating gas impurities. The WO_3 powder (supplied by BDH laboratory reagents England with a 99.99% purity) is placed in a ceramic boat and SiO_2(300 nm)/Si substrate was faced down and mounted on the top of the boat, which was located at the center inside the high-temperature zone of the tube furnace. A separate ceramic boat with sulfur powder (TTRACHEM 99 %) is placed in the lower temperature zone inside the inlet of the furnace. The temperature of the furnace is increased up to 1100°C and the deposition is carried out at the same temperature for 60 minutes under Ar gas with a rated flow of ~ 200 sccm as the carrier gas [7,31]. Figure. 2 (b) illustrates XRD patterns of the WS_2 NFs using an X-ray source at λ = 1.54 Å. The results show there is three sharp diffraction peaks at ~28.92, 43.98, and 59.90˚ attributed to the reflectance on (004), (006), and (008) crystalline surfaces related to the WS_2 NFs, respectively. The peak at about 68.91˚ is related to the silicon substrate [7].

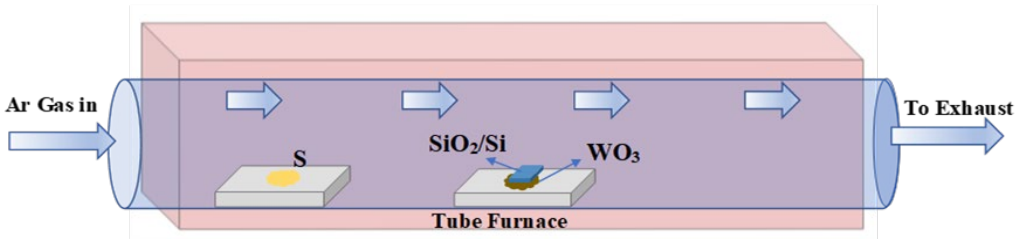

Fig. 1: Schematic of the TCVD setup for preparation of the WS2- NFs.

2.2. Preparation of the lead free perovskite $CsGeBr_3$

ssynthesis the CGB perovskite, three primal materials H_3PO_2 (50%), HBr (48%), and GeO_2 (99.998%) are mixed and heated up to120 ºC with the amount of 0.15, 0.69, and 0.001 mol for each one respectively. This mixing is continued for 6 hours and finally cooled down to room temperature (RT). After removing the remain precipitate, CSBr with amount

of 0.01 mol is added to the solution and then the temperature raised to boiling point for 5 minutes. Finally, the mixture cooled down to RT and a light-yellow precipitate is obtained. To avoid the interaction with other environmental gases, all processes are carried out under N_2 gas with a flow rate of 450 sccm. To eliminate the residual precursors, the purification is done using the solution of HBr and alcohol with a ratio of 1:1. The process for purification is repeated seven times and finally the yellow CGB precipitate is annulled at 80°C for 12 h [31-33]. Figure. 2a present the XRD patterns of CGB perovskite powder using an X-ray source at λ=1.54 Å. The pattern of CGB exhibits several crystalline orientations with two main peaks at 27.68° and 31.78° attributed to $(11\bar{1})$ and (200) planes of the orthorhombic phase [31,33]. Moreover, the presence of the impurities corresponded to the initial precursors including the CsBr and GeO_2 are observed in the pattern.

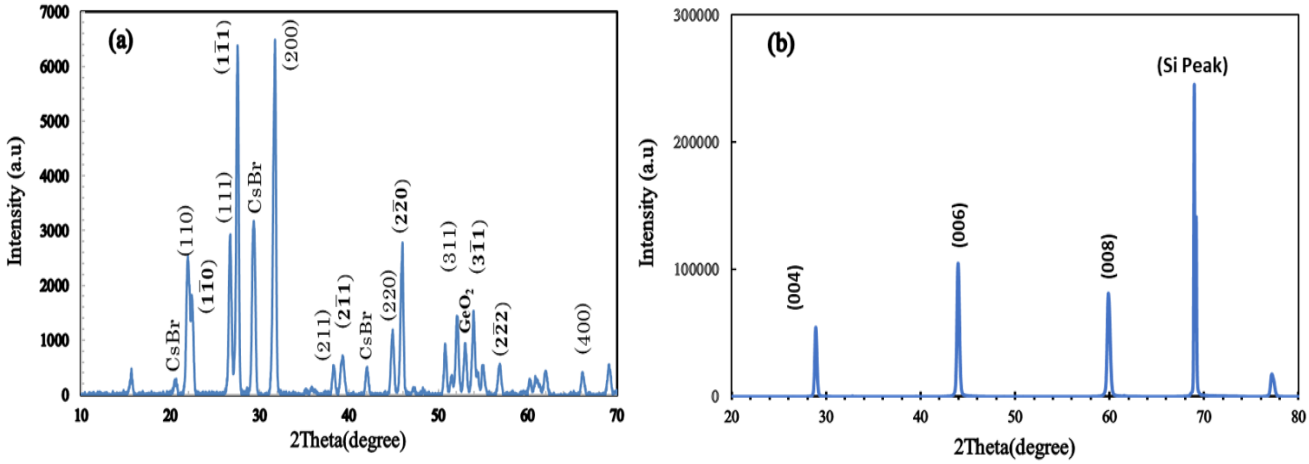

Fig. 2: XRD patterns of the a) CGB perovskite and b) WS_2 NFs [7,31-32].

2.3. Fabrication of the $CsGeBr_3/WS_2$ hybrid FET Transistor

Figure.3 contains a schematic drawing of a CGB/WS_2 NFs FET with a back-gate that is coated by CGB perovskite using the drop casting method. In order to prepare the CGB suspension, 2.5 mg of the CGB nanostructures are dispersed in 5cc ethanol by using an ultrasonic homogenizer (50 W) for 10 min. The carbon glue is used as a Two-probe measurement in this study means the standard FET measurement that has the source and the drain added with the gate, The channel width and length between the two electrodes are 10mm and 12mm, respectively.

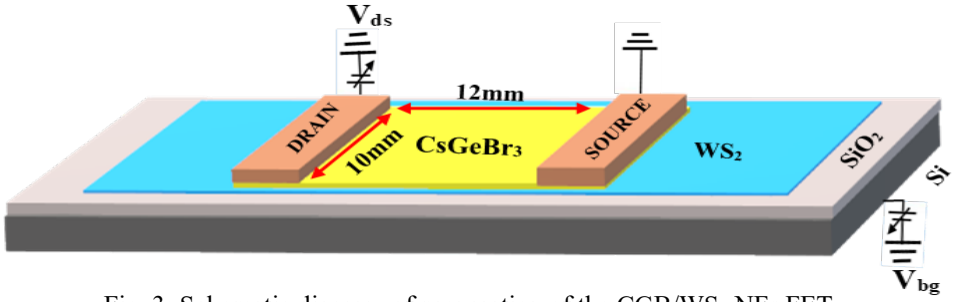

Fig. 3: Schematic diagram of preparation of the CGB/WS_2 NFs FET.

3. Result and Discussion

Figure.4 depicts the current – voltage (I_{ds}-V_{ds}) curves at different back gate voltages for fabricated transistors in air ambient and vacuum. It is clear that I_{ds}–V_{ds} curve has linear relation corresponded to the I_{ds} and V_{ds} for entire gate voltages and this linear behaviour indicates the carbon glue contact with WS_2 is ohmic in nature. According to figure.4a and figure.4b, The I_{ds} for transistors are raised by increasing the back gate voltages but the number of I_{ds} in vacuum reached around 0.13 mA for V_{bg} = 4 (V) and V_{ds} = 0.5(v) which improved in comparison with device in air ambient. It seems the increase of I_{ds} for the CGB/WS2 NFs FET in vacuum is most likely because of the removing some adsorbates from the surface of WS_2 or SiO_2/Si interface [33-34].

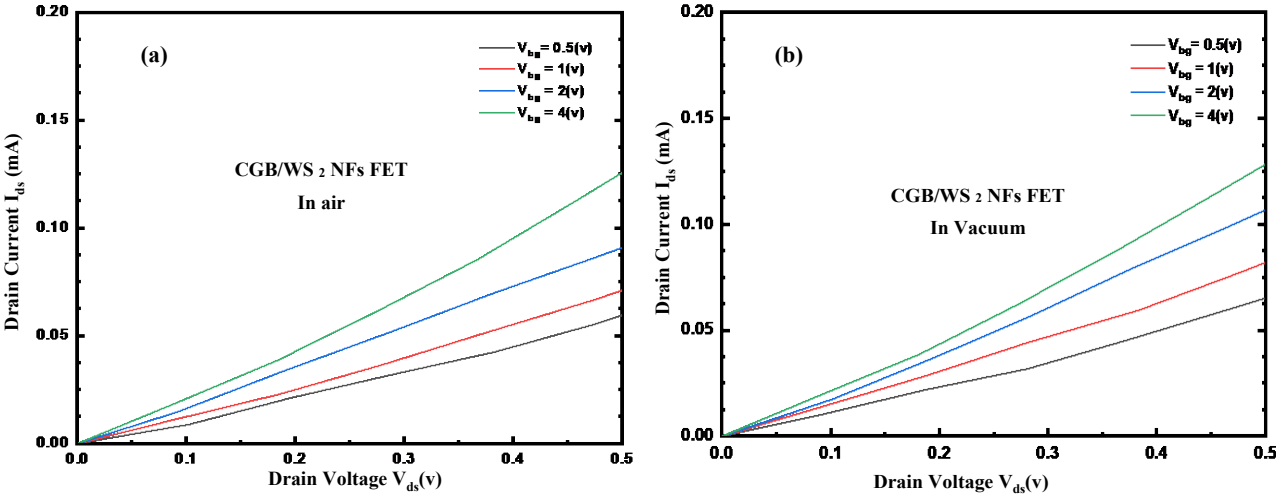

Fig. 4: Output characteristics in low source-drain bias of the WS_2–NFs in a) air ambient, and b) vacuum.

Figure.5 presents the transport characteristics (I_{ds}-V_{bg}) of transistor device for V_{bg} in the range of 0- 4v and V_{ds}=0.5v under green laser illumination for the wavelength of 455nm and illumination power =9.33mwcm^{-2}. As shown in figure, the putting the CGB/WS_2-NFs in vacuum is affected the performance of devices while the I_{ds} of transport curve is increased by positive biased voltage of V_{bg}. it is also obvious that the I_{ds} of CGB/WS_2 NFs FET of device is improved and could pass larger current by putting it in vacuum condition than air ambient for the same bias voltage then finally enhancement reached around 1.29mA at V_{bg}= 4v due to green laser illumination and finally by increasing back gate voltage. It is a sign of using the pristine chamber added the laser illumination which help charge mobility and transfer from WS_2 to $CsGeBr_3$ lead free perovskite [7,32]. The threshold voltage is defined as the intercept of the V_{bg} axis obtained by extrapolating the linear portion of the curve of I_{ds}–V_{bg} curve [35]. The inlets in figures are shown the threshold voltage (V_{th}) of CGB/WS_2 NFs FETs which are approximately 0.25V, and 0.1v in air and vacuum respectively. It observed that V_{th} is shifted toward lower voltage to 0.1v by putting the device in vacuum. In addition, the observed shift in threshold voltage suggests that atmospheric adsorbates induce substrate doping and/or trapped charge. Similar effects have also been observed on bilayer MoS_2 devices, where adsorbed oxygen and water were implicated in degraded device performance [36].

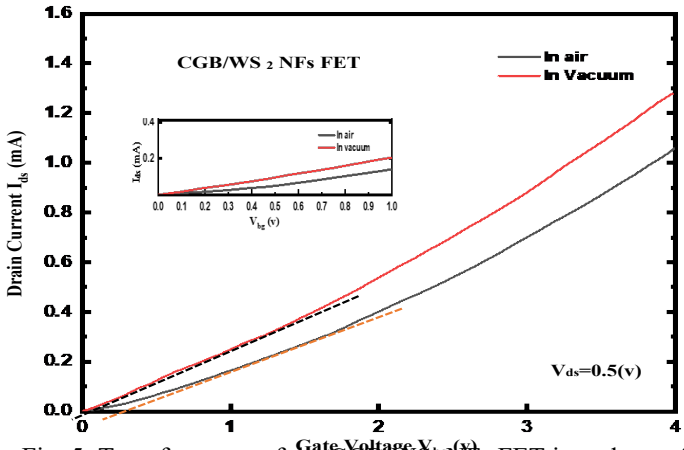

Fig. 5: Transfer curve of the CGB/WS_2-NFs FET in and out of vacuum.

To compare the performance of transistors in different situations, the Photo-responsivity (R), External Quantum Efficiency (EQE), and detectivity (D*) are calculated by using the equations (1), (2), and (3) respectively. The photo-responsivity is defined through Eqs (1):

$$R = \frac{I - I_{dark}}{A \times P} \quad (1)$$

where A, P, I, and, I_{dark} are, the area of the photoconductor, the power of the laser illumination, the measured current current under illumination, and darkness respectively [36-38]. The EQE of the photodetectors is calculated according to Equation (2):

$$EQE = \frac{R \times h \times c}{e \times \lambda} \quad (2)$$

where h, c, e, and λ are the Plank's constant, the velocity of light in a vacuum, the electronic charge, and the wavelength of the laser. The detectivity of the photodetector is calculated via Eqs (3): [7,37-38].

$$D^* = \frac{R}{((2e \times I_{dark})/A)^{1/2}} \quad (3)$$

Table 1: The EQE, D, and R comparison of the WS_2 -NFs and CGB/WS_2 NFs devices under the green laser with a wavelength of ~ 532 nm and excitation power of ~ 9.13 mwcm^{-2} at RT and V_{ds} = 1 V.

Device	R(A/W)	EQE (%)	D* (Jones)
CGB/WS_2 NFs FET (in air)	0.007	1.6	2.09×10^{-6}
CGB/WS_2 NFs FET (in vacuum)	0.012	2.9	4.15×10^{-6}

Table. 1 present the amount of EQE, D* and R parameters for CGB/WS_2 NFs device in and out of vacuum at RT. As summarized in Table. 1, the EQE, responsivity, and detectivity values of the CGB/WS_2 NFs device in vacuum approximately are doubled compared to the device in air. The maximum responsivity is also equal to 0.012 AW^{-1}, which is driven using V_{ds} at 1v related to the CGB/WS_2 NFs FET under the green laser illumination in vacuum.

4. Conclusion

In summary, the $CsGeBr_3$ perovskite was synthesized, and CGB/WS_2NFs FET was fabricated to evaluate the effect of atmosphere and vacuum on the performance of it. For each in and out of vacuum chamber, increasing the V_{bg} in transfer characteristic enhanced in the performance of the device in vacuum which detectivity, Responsivity and EQE of CGB/WS_2 NFs device was doubled in comparing the device in atmosphere. In addition, the observed shift in threshold voltage toward the lower voltage suggests that atmospheric adsorbates induce substrate doping and/or trapped charge.

References

[1] S. Assefa, F. N. A. Xia, and Y. A. Vlasov, "Reinventing germanium avalanche photodetector for nanophotonic on-chip optical interconnects," *J. Nat.,* vol. 464, no. 4, pp. 80-84, 2010.

[2] K. J. Baeg, M. Binda, D. Natali, M. Caironi, and Y. Y. Noh, "Organic light detectors: photodiodes and transistors," *J. Adv Mater*, vol. 25, no. 31, pp. 4267-4295, 2013.

[3] B. Kaviraj, and D. Sahoo, "Organic Photodiodes: The Future of Full Color Detection and Image Sensing," *J. Advanced Materials*, vol. 28, no. 24, pp. 4766-4802, 2016.

[4] J. J. Ackert, D. J. Thomson, L. Shen, A. C. Peacock, P. E. Jessop, G. T. Reed, G. Z. Mashanovich, and A. P. Knights,

"Physics of excitons and their transport in two-dimensional transition metal dichalcogenide semiconductors," *J. RSC. Adv*, vol. 9, no. 44, pp. 25439-25461, 2019.
[5] A. Venkata Krishnan, H. Chua, P. Tan, Z. H. Liu, Y. Liu, A. Carvalho, J. Lu, and C. H. Sow, "Micro steganography on WS_2 monolayers tailored by direct laser painting," *J. ACS Nano*., vol. 11, no. 1, pp. 713-720, 2015.
[6] C. C. Huang, C. L. Ho, and M. C. Wu, "Highly Uniform Photo-Sensitivity of Large-Area Planar InGaAs p-i-n Photodiodes With Low Specific Contact Resistance of Gallium Zinc Oxide," *J. IEEE Electron Device Lett*., vol. 36, no. 10, pp. 1066-1068, 2015.
[7] Y. Yue, J. Chen, Y. Zhang, S. Ding, F. Zhao, Y. Wang, D. Zhang, R. Li, H. Dong, W. Hu, Y. Feng, and W. Feng, "Two-dimensional high-quality monolayered triangular WS_2 flakes for field-effect transistors," *J. ACS Appl. Mater. Interfaces*, vol. 10, no. 26, pp. 22435-22444, 2017.
[8] C. Cong, J. Shang, Y. Wang, and T. Yub, "Optical Properties of 2D Semiconductor WS_2," *J. Adv. Optical Mater*, vol. 6, no. 4, pp. 700767, 2017.
[9] D. D. Ren, J. K. Qin, Y. Li, P. Miao, Z. Y. Sun, P. Xu, L. Zhen, and C. Y. Xu, "Photoluminescence inhomogeneity and excitons in CVD-grown monolayer," *J. Elsevier. Optical Material*, vol. 80, pp. 203-208, 2018.
[10] T. Georgiou, R Jalil, B. D. Belle, L. Britnell, R.V. Gorbachev, S.V. Morozov, Y. J. Kim, A. Gholinia, S. J. Haigh, O. Makarovsky, L. Eaves, L. A. Ponomarenko, A. K. Geim, K. S. Novoselov, and A. Mishchenko, "Vertical field-effect transistor based on graphene-WS_2 heterostructures for flexible and transparent electronics," *J. Nat. Nanotechnology*, vol. 8, no. 8, pp. 100-103, 2013.
[11] Q. H. Wang, K. Kalantar-Zadeh, A. Kis, J. N. Coleman, and M. S. Strano, "Electronics and optoelectronics of two-dimensional transition metal dichalcogenides," *J. Basic Eng*, vol. 7, no. 11, pp. 699-712, 2012.
[12] D. Braga, I. G. Lezama, H. Berger, and A. F. Morpurgo, "Quantitative Determination of the Band Gap of WS2 with Ambipolar Ionic Liquid-Gated Transistors," *J. Nano Lett*, vol. 12, no.10, pp. 5218-5223, 2012.
[13] Y. Zhang, Y. Zhang, Q. Ji, J. Ju, H. Yuan, J. Shi, T. Gao, D. Ma, M. Liu, Y. Chen, X. Song, H. Y. Hwang, Y. Cui, and Z. Liu, "Controlled growth of high-quality monolayer WS_2 layers on sapphire and imaging its grain boundary," *J. ACS Nano*, vol. 7, no. 10, pp. 8963-8971, 2013.
[14] L. Liu, S.B. Kumar, Y. Ouyang, and J. Guo, "Performance Limits of Monolayer Transition Metal Dichalcogenide Transistors," *J. IEEE Transactions on Electron Devices*, vol. 8, no. 9, pp. 3042-3047, 2011.
[15] M. Roknuzzaman, K. Ostrikov, H. Wang, A. Du, and T. Tesfamichael, "towards lead free perovskite photovoltaics and optoelectronics by ab-initio simulations," *J. Scientific reports*, vol. 7, no. 1, pp. 14025-14031, 2017.
[16] W. Deng, X. Zhang, L. Huang, X. Xu, L. Wang, J. Wang, Q. Shang, S.-T. Lee, and J. Jie, "Aligned Single-Crystalline Perovskite Microwire Arrays for High-Performance Flexible Image Sensors with Long-Term Stability," *J. Adv Mater*, vol.28, no. 11, pp. 2201-2208, 2016.
[17] M. I. Saidaminov, M. A. Haque, M. Savoie, A. L. Abdelhady, N. Cho, I. Dursun, U. Buttner, E. Alarousu, T. Wu, and O. M. Bakr, "Perovskite Photodetectors Operating in Both Narrowband and Broadband Regimes," *J. Adv Mater*, vol. 28, no. 37, pp. 8144-8149, 2016.
[18] Y. L. Guo, C. Liu, H. Tanaka, and E. Nakamura, "Air-Stable and Solution-Processable Perovskite Photodetectors for Solar-Blind UV and Visible Light," *J. Phys Chem Lett*, vol. 6, no. 3, pp. 535-539, 2015.
[19] L. Protesescu, S. Yakunin, M. I. Bodnarchuk, F. Krieg, R. Caputo, C. H. Hendon, R. X. Yang, A. Walsh, and M. V. Kovalenko, "Nanocrystals of Cesium Lead Halide Perovskites ($CsPbX_3$, X = Cl, Br, and I): Novel Optoelectronic Materials Showing Bright Emission with Wide Colour Gamut," *J. Nano Lett*, vol. 15, no. 6, pp. 3692-3696, 2015.
[20] L. Lv, Y. Xu, H. Fang, W. Luo, F. Xu, L. Liu, B. Wang, X. Zhang, D. Yang, W. Hu, and A. Dong, "Generalized colloidal synthesis of high-quality, two-dimensional cesium lead halide perovskite nanosheets and their applications in photodetectors," *J. Nanoscale*, vol. 8, no. 28, pp. 13589-13596, 2016.
[21] P. Ramasamy, D.-H. Lim, B. Kim, S.-H. Lee, M.-S. Lee, and J.-S. Lee, "All-inorganic cesium lead halide perovskite nanocrystals for photodetector applications," *J. Chem. Commun*, vol. 52, no. 10, pp. 2067-2070, 2016.
[22] X. Song, X. Liu, D. Yu, C. Huo, J. Ji, X. Li, S. Zhang, Y. Zou, G. Zhu, Y. Wang, M. Wu, A. Xie, and H. Zeng, "Boosting Two-dimensional $MoS_2/CsPbBr_3$ Photodetectors via Enhanced Light Absorbance and Interfacial Carrier Separation," *J. ACS. Appl. Mater. Interfaces*, vol. 10, no. 3, pp. 2801-2808, 2018.
[23] L. J. Chen, "Synthesis and optical properties of lead-free cesium germanium halide perovskite quantum rods," *J. RSC*

Adv, vol. 8, no. 33, pp. 18369-18399, 2018.
[24] M. H. Soltani, A. Reyhani, A. Taherkhani, S. Mirershadi, and S.Z. Mortazavi, "Efficiency enhancement of Si solar cell based on the spectral down-shifting property of $CsGeBr_3$ optimized by time and temperature of synthesis," *J. Materials in Electronics*, vol. 32, pp. 15675-15686, 2021.
[25] F. Hao, C. Stoumpos, D. H. Cao, R. P. H. Chang, and M. G. Kanatzidis, "Lead-free solid-state organic–inorganic halide perovskite solar cells," *J. Nature Photonics*, vol. 8, pp. 489-494, 2014.
[26] Z.G. Lin, L. C. Tang, and C. P. Chou, "Study on mid-IR NLO crystals CsGe $(BrxC1\text{-}x)_3$," *J. Elsevier. Optical Material*, vol. 31, pp. 28-34, 2008.
[27] F. K. Perkins, A. L. Friedman, E. Cobas, P. M. Campbell, G. G. Jernigan, and B. T. Jonker, "Chemical vapor sensing with monolayer MoS_2," *J. Nano Lett*, vol. 13, no. 2, pp. 668-673, 2013.
[28] B. Chakraborty, A. Bera, D. V. S. Muthu, S. Bhowmick, U. V. Waghmare, and A. K. Sood, "Symmetry-dependent phonon renormalization in monolayer MoS_2 transistor," *J. Phys. Rev*, vol. 85, pp. 161403, 2012.
[29] K. Kaasbjerg, K. S. Thygesen, and K. W. Jacobsen, "Phonon-Limited Mobility in n-Type Single-Layer MoS_2 from First Principles," *J. Physical review. B, Condensed matter*, vol. 85, no. 11, pp. 115317, 2012.
[30] S. Kim, A. Konar, W. Hwang, J. H. Lee, J. Lee, J. Yang, C. Jung, H. Kim, J. Yoo, J. Choi, Y. W. Jin , S. Y. Lee , D. Jena, W. Choi, and K. Kim, "High-mobility and low-power thin-film transistors based on multilayer MoS2 crystals," *J. Nature Communications*, vol. 3, pp. 1011-1018, 2012.
[31] Y. Rezaei. Nik, A. Reyhani, S. Farjami-Shayesteh, and S.Z. Mortazavi, "Photocurrent enhancement of hybrid perovskite $CsGeBr_3$ assisted two-dimensional WS_2 nano-flakes based on electron-hole mobility improvement," *J. Elsevier. Optical Material*, vol. 112, pp. 110745-110753, 2021.
[32] Z. G. Lin, L.C. Tang, and C. P. Chou, "Study on mid-IR NLO crystals CsGe $(BrxC1\text{-}x)_3$," *J. Elsevier. Optical Material*, vol. 31, pp. 28-34, 2008.
[33] Y. Rezaei. Nik, A. Reyhani, S. Farjami-Shayesteh, and S.Z. Mortazavi, A. Aghaei, A. Taherkhani "High-performance $CsGeBr_3$ perovskite/ WS_2 Nano-Flakes Field-Effect Transistor at high temperature," *J. Elsevier. Optical Material*, vol. 132, pp. 112757-112763, 2022.
[34] W. Zhang, J.K. Huang, C.H. Chen, Y.H. Chang, Y.J. Cheng, and L.J.Li, "High-Gain Transistors Based on a CVD MoS_2 Monolayer," *J. Adv. Mater*, vol. 25, pp. 3456-3461, 2013.
[35] M. W. Iqbal, M.Z. Iqbal, M. F. Khan, M.A. Shehzad, Y. Seo, J.H. Park, C. Hwang, and J. Eom, "High-mobility and air-stable single layer WS_2 field-effect transistors sandwiched between chemical vapor deposition-grown hexagonal BN films," *J. Scientific Reports*, vol. 5, pp. 10699, 2015.
[36] D. Jariwala, V.K. Sangwan, D. J. Late, J.E. Johns, V.P. Dravid, T. J. Marks, L.J. Lauhon, and M. C. Hersam, "Band like transport in high mobility unencapsulated single-layer MoS_2 transistors," *J. AIP*, vol. 102, no. 17, pp. 173107-13111, 2013.
[37] N. Islam, M. A. Hadi, and J. Podder, "Influence of Ni doping in a lead-halide and a lead-free halide perovskite for optoelectronic applications," *J. AIP Advances*, vol. 9, no. 12, pp. 125321, 2019.
[38] Y. Zhao, and K. Z.hu, "Organic–inorganic hybrid lead halide perovskites for optoelectronic and electronic applications," *J. Chem. Soc. Rev*, vol. 45, no. 3, pp. 665-689, 2016.